

HIERARCHICAL INTERPOLATIVE FACTORIZATION FOR ELLIPTIC OPERATORS: INTEGRAL EQUATIONS

KENNETH L. HO AND LEXING YING

ABSTRACT. This paper introduces the hierarchical interpolative factorization (HIF) for integral operators associated with elliptic partial differential equations in 2D and 3D. The HIF is an approximate multilevel factorization that diagonalizes the matrix discretization of the operator through a sequence of triangular transformations. As such, it is also easily invertible. The HIF is based on the recursive skeletonization method but uses additional levels of compression via dimensional reductions to control the rank growth. Thus, algorithms to construct, apply, and invert the HIF all have essentially linear cost. Numerical results in both 2D and 3D demonstrate its efficiency as a fast multipole method, direct solver, and preconditioner. The HIF is applicable to both boundary and volume problems.

1. INTRODUCTION

This paper considers integral equations of the form

$$(1.1) \quad a(x)u(x) + b(x) \int_{\Omega} K(\|x - y\|)c(y)u(y) d\Omega(y) = f(x), \quad x \in \Omega \subset \mathbb{R}^d$$

associated with elliptic partial differential equations (PDEs), where $a(x)$, $b(x)$, $c(x)$, and $f(x)$ are given functions, the integral kernel $K(r)$ is related to the fundamental solution of the PDE, and $d = 2$ or 3 . Such equations encompass both boundary and volume problems and can be derived from PDEs in various ways. We give two prototypical examples below:

(1) Consider the Dirichlet Laplace problem

$$(1.2a) \quad \Delta u(x) = 0, \quad x \in \Omega,$$

$$(1.2b) \quad u(x) = f(x), \quad x \in \partial\Omega \equiv \Gamma,$$

which can be solved by writing u as the double-layer potential

$$(1.3) \quad u(x) = \int_{\Gamma} \frac{\partial K}{\partial \nu_y}(\|x - y\|)\sigma(y) d\Gamma(y), \quad x \in \Omega$$

over an unknown surface density σ , where

$$(1.4) \quad K(r) = \begin{cases} -1/(2\pi) \log r, & d = 2, \\ 1/(4\pi r), & d = 3 \end{cases}$$

is the fundamental solution of the free-space PDE and ν_y is the unit outer normal at $y \in \Gamma$. Clearly, (1.3) satisfies (1.2a). To enforce the boundary condition (1.2b), take the limit as $x \rightarrow \Gamma$ and use standard results from potential theory [28] to obtain

$$(1.5) \quad -\frac{1}{2}\sigma(x) + \int_{\Gamma} \frac{\partial K}{\partial \nu_y}(\|x - y\|)\sigma(y) d\Gamma(y) = f(x), \quad x \in \Gamma,$$

where the integral is defined in the principal value sense. This is a boundary integral equation for $\sigma(x)$ of the form (1.1).

Alternatively, we could use the single-layer potential representation

$$u(x) = \int_{\Gamma} K(\|x - y\|)\sigma(y) d\Gamma(y), \quad x \in \Omega,$$

which immediately gives the integral equation

$$\int_{\Gamma} K(\|x - y\|)\sigma(y) d\Gamma(y) = f(x), \quad x \in \Gamma$$

upon taking the limit $x \rightarrow \Gamma$ since the integral is well-defined. Note that this has $a(x) \equiv 0$ in (1.1). Such equations are called first-kind integral equations and are ill-conditioned. Second-kind integral equations such as (1.5), on the other hand, have $a(x) \neq 0$ for all x and are generally well-conditioned.

(2) Consider the divergence-form PDE

$$\nabla \cdot (a(x)\nabla u(x)) = f(x), \quad x \in \Omega$$

and let

$$u(x) = \int_{\Omega} K(\|x - y\|)\sigma(y) d\Omega(y),$$

where $K(r)$ is as defined in (1.4). Then the PDE becomes

$$a(x)\sigma(x) + \nabla a(x) \cdot \int_{\Omega} \nabla_x K(\|x - y\|)\sigma(y) d\Omega(y) = f(x).$$

Integral equations can similarly be derived for many of the PDEs of classical physics including the Laplace, Helmholtz, Stokes, and time-harmonic Maxwell equations. In such cases, the kernel function $K(r)$ is typically singular near zero but otherwise smooth. For this paper, we will also require that $K(r)$ not be too oscillatory.

Discretization of (1.1) using, e.g., the Nyström, collocation, or Galerkin method leads to a linear system

$$(1.6) \quad Au = f,$$

where $A \in \mathbb{C}^{N \times N}$ is dense with u and f the discrete analogues of $u(x)$ and $f(x)$, respectively. This paper is concerned with the efficient factorization and solution of such systems.

1.1. Previous work. Numerical methods for solving (1.6) can be classified into several groups. The first consists of classical direct methods like Gaussian elimination or other standard matrix factorizations [23], which compute the solution exactly (to machine precision) without iteration. These methods are useful when N is small. However, since A is dense, the $\mathcal{O}(N^3)$ complexity quickly makes them infeasible as N increases.

The second group is that of iterative methods [44], among the most popular of which are Krylov subspace methods such as conjugate gradient [33, 48] or GMRES [45]. The number of iterations required depends on the problem and is typically small for second-kind integral equations but can grow rapidly for first-kind ones. The main computational cost is the calculation of matrix-vector products at each iteration. Combined with fast multipole methods (FMMs) [19, 25, 26, 52] or other accelerated multiplication algorithms [2, 31, 43], such techniques can yield asymptotically optimal or near-optimal solvers with $\mathcal{O}(N)$ or $\mathcal{O}(N \log N)$ complexity. However, iterative methods are often not as robust as their direct counterparts, especially when $a(x)$, $b(x)$, or $c(x)$ lacks regularity or has high contrast. Furthermore, iterative methods can be inefficient for systems with multiple right-hand sides, which is an important setting for many applications of interest.

The third group covers rank-structured direct solvers, which are based on the observation that the off-diagonal blocks of A and A^{-1} are numerically low-rank. The seminal work in this area is by Hackbusch et al. [29, 30], whose \mathcal{H} - and \mathcal{H}^2 -matrices have been shown to provide essentially linear complexity in certain cases [5]. However, the prefactor can be large due to the need for expensive hierarchical matrix-matrix multiplication.

More recent developments include solvers for hierarchically semiseparable matrices [1, 10, 11, 50] and methods based on recursive skeletonization (RS) [22, 24, 35, 39], among other related techniques [6, 12]. These are optimal in 1D but have superlinear complexities in 2D and 3D. In particular, RS proceeds very similarly to the nested dissection multifrontal method for sparse linear systems [16], with the so-called skeletons characterizing the off-diagonal matrix blocks corresponding to the separator fronts. These grow as $\mathcal{O}(N^{1/2})$ in 2D and $\mathcal{O}(N^{2/3})$ in 3D, resulting in solver complexities of $\mathcal{O}(N^{3/2})$ and $\mathcal{O}(N^2)$, respectively, for factorization and $\mathcal{O}(N \log N)$ and $\mathcal{O}(N^{4/3})$, respectively, for the solve time and memory required. Recently, Corona et al. [15] reported an $\mathcal{O}(N)$ RS solver in 2D by using hierarchical matrix algebra on the skeletons themselves. However, this approach has yet to be realized in 3D or in complicated domains.

1.2. Contributions. In this paper, we introduce the hierarchical interpolative factorization (HIF) for integral operators, which builds upon the RS scheme. Much like RS (though it has not traditionally been presented in this way), it diagonalizes the matrix A (to a specified precision) through a sequence of triangular transformations. As such, it is also easily invertible. The primary novelty of the HIF is that the skeleton/separator structure can be further compressed, in particular that the rank growth in 2D and 3D can be suppressed through dimensional reductions via geometric clustering and additional skeletonization. Thus, algorithms to construct, apply, and invert the HIF all have essentially linear cost. The HIF is applicable to both boundary and volume problems in 2D and 3D, and can be used as an FMM, direct solver, or preconditioner.

1.3. Outline. The remainder of this paper is organized as follows. Section 2 introduces the notation and basic building blocks of our approach. The main section, Section 3, describes the algorithm in detail in both 2D and 3D, complete with complexity estimates. Several numerical examples are given in Section 4. Finally, Section 5 concludes with some discussion and future directions.

2. PRELIMINARIES

In this section, we first list our notational conventions and then describe the main tools behind the HIF.

2.1. Notation. The uppercase letters $A, B, D, F, Q, R, S, T, U$, and V are used to denote matrices. The lowercase letters c, p, q, r , and w denote row or column degrees of freedom (DOFs) of a matrix. For a given DOF set c , its cardinality is given by $|c|$. The uppercase letter C denotes a collection of disjoint DOF sets. The complement of a DOF set c is written c^C , with the parent set to be understood from the context.

Given a matrix A , A_{pq} is the submatrix with rows and columns restricted to the DOF sets p and q , respectively. We also use the MATLAB notation $A_{:,q}$ to denote the submatrix with columns only restricted to q .

2.2. Schur complement. Let

$$A = \begin{bmatrix} A_{pp} & A_{pq} & \\ A_{qp} & A_{qq} & A_{qr} \\ & A_{rq} & A_{rr} \end{bmatrix}$$

be a matrix defined over the DOFs $p \cup q \cup r$ with p , q , and r disjoint (possibly empty). The essence of the Schur complement is to use block row and column operations to decouple the DOFs p from the rest. Assume that A_{pp} is nonsingular and define

$$R_p^* = \begin{bmatrix} I & & \\ -A_{qp}A_{pp}^{-1} & I & \\ & & I \end{bmatrix}, \quad S_p = \begin{bmatrix} I & -A_{pp}^{-1}A_{pq} & \\ & I & \\ & & I \end{bmatrix}.$$

Then

$$R_p^*AS_p = \begin{bmatrix} A_{pp} & & \\ & A_{qq} - A_{qp}A_{pp}^{-1}A_{pq} & A_{qr} \\ & A_{rq} & A_{rr} \end{bmatrix}$$

so that p has been eliminated. Note that the DOFs r not interacting with p are unaffected.

2.3. Interpolative decomposition. Let A be a low-rank matrix with column DOFs q . Then there exists a subset \hat{q} of columns such that any other column of A can be expressed as a linear combination of $A_{:, \hat{q}}$. More specifically, q has a partitioning $q = \check{q} \cup \hat{q}$ in terms of *redundant* and *skeleton* columns \check{q} and \hat{q} , respectively, such that

$$(2.1) \quad A_{:, \check{q}} = A_{:, \hat{q}}T_q,$$

where $\|T_q\|$ is typically small. This factorization is called the *interpolative decomposition* (ID) [13] and is generally not unique.

If A is low-rank only to a specified numerical precision, as is common when A is the discretization of an integral operator acting between separated spatial regions [24, 35], then an ID exists such that (2.1) holds to any relative precision $\epsilon > 0$.

The ID can be computed robustly using a rank-revealing QR factorization [9, 27]. This can be expensive, however, so a pivoted QR factorization [23] is often used in practice, with the pivot threshold controlling the approximation error. Fast algorithms based on random sampling are also available [32, 38, 41, 49], but we use only the standard pivoted QR in this paper.

2.4. Skeletonization. We now combine the ID with the Schur complement to decouple redundant DOFs. Let

$$(2.2) \quad A = \begin{bmatrix} A_{pp} & A_{pq} \\ A_{qp} & A_{qq} \end{bmatrix}$$

be a matrix defined over the DOFs $p \cup q$ with p and q disjoint, and assume that the off-diagonal blocks $A_{p^c, p} = A_{qp}$ and $A_{q^c, q} = A_{pq}$ are numerically low-rank. Then applying the ID to $A_{p^c, p}$ and A_{p, p^c}^* together (with respect to p) gives the approximation

$$\begin{bmatrix} A_{p^c, \check{p}} \\ A_{\check{p}, p^c}^* \end{bmatrix} \approx \begin{bmatrix} A_{p^c, \hat{p}} \\ A_{\hat{p}, p^c}^* \end{bmatrix} T_p,$$

i.e.,

$$A_{p^c, \check{p}} \approx A_{p^c, \hat{p}}T_p, \quad A_{\check{p}, p^c} \approx T_p^*A_{\hat{p}, p^c},$$

and similarly for q . Without loss of generality, let

$$A = \begin{bmatrix} A_{\check{p}\check{p}} & A_{\check{p}\hat{p}} & A_{\check{p}\check{q}} & A_{\check{p}\hat{q}} \\ A_{\hat{p}\check{p}} & A_{\hat{p}\hat{p}} & A_{\hat{p}\check{q}} & A_{\hat{p}\hat{q}} \\ A_{\check{q}\check{p}} & A_{\check{q}\hat{p}} & A_{\check{q}\check{q}} & A_{\check{q}\hat{q}} \\ A_{\hat{q}\check{p}} & A_{\hat{q}\hat{p}} & A_{\hat{q}\check{q}} & A_{\hat{q}\hat{q}} \end{bmatrix}$$

and notice that

$$\begin{bmatrix} I & -T_p^* \\ & I \end{bmatrix} \begin{bmatrix} A_{\tilde{p}\tilde{q}} & A_{\tilde{p}\hat{q}} \\ A_{\hat{p}\tilde{q}} & A_{\hat{p}\hat{q}} \end{bmatrix} \begin{bmatrix} I & \\ -T_q & I \end{bmatrix} \approx \begin{bmatrix} I & -T_p^* \\ & I \end{bmatrix} \begin{bmatrix} T_p^* \\ I \end{bmatrix} A_{\hat{p}\hat{q}} \begin{bmatrix} T_q & I \\ -T_q & I \end{bmatrix} = \begin{bmatrix} 0 & 0 \\ 0 & A_{\hat{p}\hat{q}} \end{bmatrix}.$$

Hence, introducing the matrices

$$Q_p = \begin{bmatrix} I & & & \\ -T_p & I & & \\ & & I & \\ & & & I \end{bmatrix}, \quad Q_q = \begin{bmatrix} I & & & \\ & I & & \\ & & I & \\ & & & -T_q & I \end{bmatrix},$$

which we remark are not unitary, we find that

$$(2.3) \quad Q_q^* Q_p^* A Q_p Q_q \approx \begin{bmatrix} B_{\tilde{p}\tilde{p}} & B_{\tilde{p}\hat{p}} & & \\ B_{\hat{p}\tilde{p}} & A_{\hat{p}\hat{p}} & & A_{\hat{p}\hat{q}} \\ & & B_{\tilde{q}\tilde{q}} & B_{\tilde{q}\hat{q}} \\ & & A_{\hat{q}\tilde{p}} & B_{\hat{q}\hat{q}} \end{bmatrix},$$

where

$$\begin{aligned} B_{\tilde{p}\tilde{p}} &= A_{\tilde{p}\tilde{p}} - T_p^* A_{\tilde{p}\hat{p}} - A_{\tilde{p}\tilde{p}} T_p + T_p^* A_{\hat{p}\tilde{p}} T_p, \\ B_{\hat{p}\tilde{p}} &= A_{\tilde{p}\hat{p}} - T_p^* A_{\hat{p}\tilde{p}}, \\ B_{\tilde{p}\hat{p}} &= A_{\hat{p}\tilde{p}} - A_{\hat{p}\tilde{p}} T_p, \end{aligned}$$

and similarly for the matrices associated with q . Note that \tilde{p} now interacts only with \hat{p} and \tilde{q} only with \hat{q} . Assuming that $B_{\tilde{p}\tilde{p}}$ and $B_{\tilde{q}\tilde{q}}$ are nonsingular, we can apply the Schur complement matrices

$$(2.4) \quad R_p^* = \begin{bmatrix} I & & & \\ -B_{\tilde{p}\tilde{p}}^{-1} B_{\tilde{p}\hat{p}} & I & & \\ & & I & \\ & & & I \end{bmatrix}, \quad S_p = \begin{bmatrix} I & -B_{\tilde{p}\tilde{p}}^{-1} B_{\tilde{p}\hat{p}} & & \\ & I & & \\ & & I & \\ & & & I \end{bmatrix},$$

and similarly for q , to obtain

$$(2.5) \quad R_q^* R_p^* Q_q^* Q_p^* A Q_p Q_q S_p S_q \approx \begin{bmatrix} B_{\tilde{p}\tilde{p}} & & & \\ & B_{\hat{p}\hat{p}} & & A_{\hat{p}\hat{q}} \\ & & B_{\tilde{q}\tilde{q}} & \\ & A_{\hat{q}\tilde{p}} & & B_{\hat{q}\hat{q}} \end{bmatrix},$$

where

$$B_{\tilde{p}\hat{p}} = A_{\tilde{p}\hat{p}} - B_{\tilde{p}\tilde{p}}^{-1} B_{\tilde{p}\tilde{p}} B_{\tilde{p}\hat{p}}, \quad B_{\tilde{q}\hat{q}} = A_{\tilde{q}\hat{q}} - B_{\tilde{q}\tilde{q}}^{-1} B_{\tilde{q}\tilde{q}} B_{\tilde{q}\hat{q}}.$$

The result is that the redundant DOFs $\tilde{p} \cup \tilde{q}$ are decoupled from the rest, with the interaction between \hat{p} and \hat{q} unmodified. This whole procedure of generating the right-hand side of (2.5) is called *skeletonization*. We denote the result by $\mathcal{Z}(A)$, which is significantly sparsified.

In this paper, we often work with a collection of disjoint DOF sets $C = \{c\}$, where $A_{c,c}$ and $A_{c,c}$ are numerically low-rank. Applying the above for all $c \in C$ gives

$$\mathcal{Z}(A) \approx U^* A V, \quad U = \prod_{c \in C} Q_c \prod_{c \in C} R_c = \prod_{c \in C} Q_c R_c, \quad V = \prod_{c \in C} Q_c \prod_{c \in C} S_c = \prod_{c \in C} Q_c S_c,$$

where the DOFs $\bigcup_{c \in C} \tilde{c}$ are decoupled from the rest and the product over C can be taken in any order. When there is a need to distinguish among multiple collections, C_ℓ and \mathcal{Z}_ℓ are used to denote a specific collection and its skeletonization operator, respectively.

3. ALGORITHM

The combination of skeletonization and a hierarchical geometric ordering such as a quadtree in 2D or an octree in 3D [46] leads to an RS solver [22, 24, 35, 39]. At each level, the skeleton DOFs tend to line the interfaces between geometric groups. Therefore, $|\hat{c}| = \mathcal{O}(N^{1/2})$ in 2D and $\mathcal{O}(N^{2/3})$ in 3D, resulting in solver complexities of $\mathcal{O}(N^{3/2})$ and $\mathcal{O}(N^2)$, respectively, as discussed in Section 1. However, the interface configuration possesses considerable structure, in particular that any two interfaces are separated so their interaction is low-rank. This observation was exploited in [15], which used hierarchical matrix operations along the interfaces to build an $\mathcal{O}(N)$ solver in 2D.

Here, we proceed slightly differently by explicitly skeletonizing the interfaces via an appropriate reordering of the remaining DOFs. Thus, we reduce each interface to its minimal size before proceeding to the next level. This keeps all intermediate matrices small so that no hierarchical matrix operations are required; only highly efficient dense linear algebra is used.

In the remainder of this section, we describe the HIF, which performs this process of recursively “skeletonizing the skeletons” down in dimension. Algorithms are given in both 2D and 3D, with complexity estimates for each.

3.1. Two dimensions. Consider the integral equation (1.1) on $\Omega = (0, 1)^2$, discretized using a piecewise constant collocation method over a uniform grid for simplicity. More general domains and discretizations can be handled without difficulty, but the current setting will serve to illustrate the main ideas. Let h be the step size in each direction and assume that $n = 1/h = 2^L m$, where $m = \mathcal{O}(1)$ is a small integer. Integer pairs $j = (j_1, j_2)$ index the elements $\Omega_j = ((j_1 - 1)h, j_1 h) \times ((j_2 - 1)h, j_2 h)$ and their centers $x_j = ((j_1 - 1/2)h, (j_2 - 1/2)h)$ for $1 \leq j_1, j_2 \leq n$. With $\{x_j\}$ as the collocation points, the discrete system (1.6) reads

$$a_i u_i + b_i \sum_j K_{ij} c_j u_j = f_i$$

for each i with $x_i \in \Omega$, where $a_j = a(x_j)$, $b_j = b(x_j)$, $c_j = c(x_j)$, and $f_j = f(x_j)$; u_j is the approximation to $u(x_j)$; and

$$K_{ij} = K(\|x_i - x_j\|)h^2, \quad i \neq j$$

with

$$K_{ii} = \int_{\Omega_i} K(\|x_i - y\|) dy$$

on the diagonal. Note that A is not stored since it is dense; rather, its entries are generated as needed. The total number of DOFs is $N = n^2 = 2^{2L}$.

The algorithm proceeds by decoupling DOFs level by level. At each level ℓ , the set of DOFs that have not been decoupled are called *active* and denoted by w_ℓ . Initially, we set $A_0 = A$ and let w_0 be the set of all DOFs. Figure 3.1 provides a schematic overview of the algorithm.

Level 0. Defined at this point are A_0 and w_0 . There are $2^L \times 2^L$ squares of width mh , each containing m^2 active DOFs. Let $C_0 = \{c\}$ be the disjoint collection of all such DOFs, where each c is the set of DOFs of one square. Clearly, $\bigcup_{c \in C_0} c = w_0$. Then skeletonization with respect to C_0 gives

$$A_{1/2} = \mathcal{Z}_0(A_0) \approx U_0^* A_0 V_0, \quad U_0 = \prod_{c \in C_0} Q_c R_c, \quad V_0 = \prod_{c \in C_0} Q_c S_c,$$

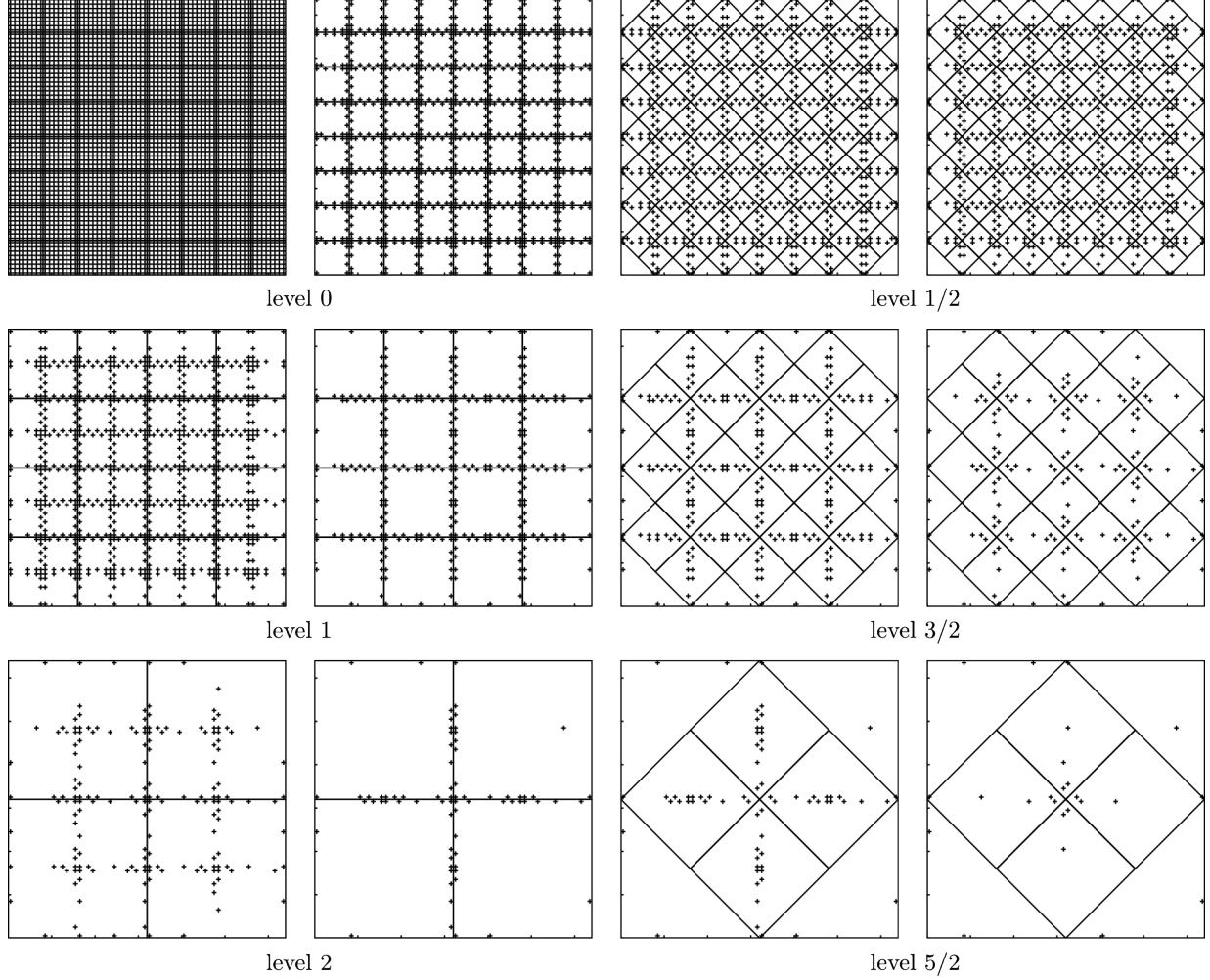


FIGURE 3.1. Schematic of the HIF in 2D, showing the active DOFs before and after each level of skeletonization along with all cell boundaries. The final level $L = 3$ consists of a single cell containing all remaining DOFs and is not displayed.

where the DOFs $\bigcup_{c \in C_0} \check{c}$ have been decoupled (and marked inactive). Let $w_{1/2} = w_0 \setminus \bigcup_{c \in C_0} \check{c} = \bigcup_{c \in C_0} \hat{c}$ be the remaining active DOFs. Then $A_{1/2}$ is block diagonal with block partitioning

$$\pi_{1/2} = \left\{ \bigcup_{c \in C_0} \hat{c}, w_{1/2} \right\}.$$

Level 1/2. Defined at this point are $A_{1/2}$ and $w_{1/2}$, with the active DOFs lying along the edges of the squares of width mh from level 0. We construct a Voronoi diagram on the edge centers. The resulting cells partition $w_{1/2}$ into a disjoint collection $C_{1/2} = \{c\}$, where each c is the set of active DOFs of one such cell. Clearly, $\bigcup_{c \in C_{1/2}} c = w_{1/2}$. Skeletonization with respect to $C_{1/2}$ then yields

$$A_1 = \mathcal{Z}_{1/2}(A_{1/2}) \approx U_{1/2}^* A_{1/2} V_{1/2}, \quad U_{1/2} = \prod_{c \in C_{1/2}} Q_c R_c, \quad V_{1/2} = \prod_{c \in C_{1/2}} Q_c S_c,$$

where the DOFs $\bigcup_{c \in C_{1/2}} \check{c}$ have been decoupled. Let $w_1 = w_{1/2} \setminus \bigcup_{c \in C_{1/2}} \check{c} = \bigcup_{c \in C_{1/2}} \hat{c}$ be the remaining active DOFs. Then A_1 is block diagonal with block partitioning

$$\pi_1 = \left\{ \bigcup_{c \in C_0} \check{c}, \bigcup_{c \in C_{1/2}} \check{c}, w_1 \right\}.$$

Note that the interactions compressed at this level do not generally correspond to those of the original kernel. This is because skeletonization at level 0 modifies the self-interactions within each DOF set $\hat{c} \in C_0$ according to (2.5). However, it has been observed numerically that such modified kernels can also be compressed [15]. Thus, they behave essentially just like the original kernel and we will make no further distinction between them in this regard.

In truth, the situation is actually slightly more complicated as we have to compress a mixture of the original and a modified kernel since for each DOF in $c \in C_{1/2}$ belonging to a given cell at level 0, $c^c \in C_{1/2}$ contains DOFs both inside and outside that cell. Nevertheless, our results suggest that this poses no difficulty and that the entire kernel mixture can, in fact, be treated just like the original kernel.

The end result is that A_1 is significantly sparsified, with the remaining active DOFs w_1 clustered about the points at which the edges meet.

Level ℓ . Defined at this point are A_ℓ and w_ℓ . There are $2^{L-\ell} \times 2^{L-\ell}$ squares of width $2^\ell mh$. Let $C_\ell = \{c\}$ be the disjoint collection of the active DOFs c of each square. Clearly, $\bigcup_{c \in C_\ell} c = w_\ell$. Skeletonization with respect to C_ℓ gives

$$A_{\ell+1/2} = \mathcal{Z}_\ell(A_\ell) \approx U_\ell^* A_\ell V_\ell, \quad U_\ell = \prod_{c \in C_\ell} Q_c R_c, \quad V_\ell = \prod_{c \in C_\ell} Q_c S_c,$$

where the DOFs $\bigcup_{c \in C_\ell} \check{c}$ have been decoupled. The matrix $A_{\ell+1/2}$ is block diagonal with block partitioning

$$\pi_{\ell+1/2} = \left\{ \bigcup_{c \in C_0} \check{c}, \bigcup_{c \in C_{1/2}} \check{c}, \dots, \bigcup_{c \in C_\ell} \check{c}, w_{\ell+1/2} \right\},$$

where $w_{\ell+1/2} = w_\ell \setminus \bigcup_{c \in C_\ell} \check{c} = \bigcup_{c \in C_\ell} \hat{c}$.

Level $\ell + 1/2$. Defined at this point are $A_{\ell+1/2}$ and $w_{\ell+1/2}$. We construct a Voronoi diagram on the centers of the edges of the squares of width $2^\ell mh$. The resulting cells partition $w_{\ell+1/2}$ into a disjoint collection $C_{\ell+1/2} = \{c\}$, where each c is the set of active DOFs of one such cell. Clearly, $\bigcup_{c \in C_{\ell+1/2}} c = w_{\ell+1/2}$. Skeletonization with respect to $C_{\ell+1/2}$ gives

$$A_{\ell+1} = \mathcal{Z}_{\ell+1/2}(A_{\ell+1/2}) \approx U_{\ell+1/2}^* A_{\ell+1/2} V_{\ell+1/2}, \quad U_{\ell+1/2} = \prod_{c \in C_{\ell+1/2}} Q_c R_c, \quad V_{\ell+1/2} = \prod_{c \in C_{\ell+1/2}} Q_c S_c,$$

where the DOFs $\bigcup_{c \in C_{\ell+1/2}} \check{c}$ have been decoupled. The matrix $A_{\ell+1}$ is block diagonal with block partitioning

$$\pi_{\ell+1} = \left\{ \bigcup_{c \in C_0} \check{c}, \bigcup_{c \in C_{1/2}} \check{c}, \dots, \bigcup_{c \in C_{\ell+1/2}} \check{c}, w_{\ell+1} \right\},$$

where $w_{\ell+1} = w_{\ell+1/2} \setminus \bigcup_{c \in C_{\ell+1/2}} \check{c} = \bigcup_{c \in C_{\ell+1/2}} \hat{c}$.

Level L. Finally, we have A_L and w_L , where $D \equiv A_L$ is block diagonal with block partitioning

$$\pi_L = \left\{ \bigcup_{c \in C_0} \check{c}, \bigcup_{c \in C_{1/2}} \check{c}, \dots, \bigcup_{c \in C_{L-1/2}} \check{c}, w_L \right\}.$$

Combining the approximation over all levels gives

$$D \approx U_{L-1/2}^* \cdots U_{1/2}^* U_0^* A V_0 V_{1/2} \cdots V_{L-1/2},$$

so

$$(3.1a) \quad A \approx U_0^{-*} U_{1/2}^{-*} \cdots U_{L-1/2}^{-*} D V_{L-1/2}^{-1} \cdots V_{1/2}^{-1} V_0^{-1} \equiv F,$$

$$(3.1b) \quad A^{-1} \approx V_0 V_{1/2} \cdots V_{L-1/2} D^{-1} U_{L-1/2}^* \cdots U_{1/2}^* U_0^* = F^{-1}.$$

Note that U_ℓ and V_ℓ are products of triangular matrices, each of which can be inverted simply by negating its off-diagonal entries. The factorization F allows fast multiplication and therefore can be used as a kernel-independent FMM. Its inverse F^{-1} can be used as a direct solver at high precision or as a preconditioner at low precision. We emphasize that F and F^{-1} are never formed explicitly and are applied only in factored form.

Remark 3.1. In this framework, RS uses only the integer levels $\ell = 0, 1, \dots, L$ above. Therefore, the HIF is a direct extension of RS, supplementing it with fractional levels of additional skeletonization.

3.2. Three dimensions. We now consider the integral equation (1.1) on $\Omega = (0, 1)^3$, similarly discretized via a piecewise constant collocation method over a uniform grid. As in 2D, this model problem is not restrictive; see Example 4 in Section 4.2, for instance, for an application to a boundary value problem. Again, let h be the step size in each direction and assume that $n = 1/h = 2^L m$, where $m = \mathcal{O}(1)$ is a small integer. Integer triplets $j = (j_1, j_2, j_3)$ index the elements $\Omega_j = ((j_1 - 1)h, j_1 h) \times ((j_2 - 1)h, j_2 h) \times ((j_3 - 1)h, j_3 h)$ and their centers $x_j = ((j_1 - 1/2)h, (j_2 - 1/2)h, (j_3 - 1/2)h)$ for $1 \leq j_1, j_2, j_3 \leq n$. With $\{x_j\}$ as the collocation points, the discrete system (1.6) reads

$$a_i u_i + b_i \sum_j K_{ij} c_j u_j = f_i$$

for each i with $x_i \in \Omega$, where $a_j = a(x_j)$, $b_j = b(x_j)$, $c_j = c(x_j)$, and $f_j = f(x_j)$; u_j is the approximation to $u(x_j)$; and

$$K_{ij} = K(\|x_i - x_j\|) h^3, \quad i \neq j$$

with

$$K_{ii} = \int_{\Omega_i} K(\|x_i - y\|) dy$$

on the diagonal. Note that A is not stored since it is dense. The total number of DOFs is $N = n^3 = 2^{3L}$.

As in 2D, the algorithm decouples DOFs level by level but with an additional reduction to account for the extra dimension. Initially, we set $A_0 = A$ and let w_0 be the set of all DOFs.

Level 0. Defined at this point are A_0 and w_0 . There are $2^L \times 2^L \times 2^L$ cubes of width mh , each containing m^3 active DOFs. Let $C_0 = \{c\}$ be the disjoint collection of all such DOFs, where each c is the set of DOFs of one cube. Clearly, $\bigcup_{c \in C_0} c = w_0$. Then skeletonization with respect to C_0 gives

$$A_{1/3} = \mathcal{Z}_0(A_0) \approx U_0^* A_0 V_0, \quad U_0 = \prod_{c \in C_0} Q_c R_c, \quad V_0 = \prod_{c \in C_0} Q_c S_c,$$

where the DOFs $\bigcup_{c \in C_0} \check{c}$ have been decoupled (and marked inactive). Let $w_{1/3} = w_0 \setminus \bigcup_{c \in C_0} \check{c} = \bigcup_{c \in C_0} \hat{c}$ be the remaining active DOFs. Then $A_{1/3}$ is block diagonal with block partitioning

$$\pi_{1/3} = \left\{ \bigcup_{c \in C_0} \check{c}, w_{1/3} \right\}.$$

Level 1/3. Defined at this point are $A_{1/3}$ and $w_{1/3}$, with the active DOFs lying along the faces of the cubes of width mh from level 0. We construct a Voronoi diagram on the face centers. The resulting cells partition $w_{1/3}$ into a disjoint collection $C_{1/3} = \{c\}$, where each c is the set of active DOFs of one such cell. Clearly, $\bigcup_{c \in C_{1/3}} c = w_{1/3}$. Skeletonization with respect to $C_{1/3}$ then yields

$$A_{2/3} = \mathcal{Z}_{1/3}(A_{1/3}) \approx U_{1/3}^* A_{1/3} V_{1/3}, \quad U_{1/3} = \prod_{c \in C_{1/3}} Q_c R_c, \quad V_{1/3} = \prod_{c \in C_{1/3}} Q_c S_c,$$

where the DOFs $\bigcup_{c \in C_{1/3}} \check{c}$ have been decoupled. Let $w_{2/3} = w_{1/3} \setminus \bigcup_{c \in C_{1/3}} \check{c} = \bigcup_{c \in C_{1/3}} \hat{c}$ be the remaining active DOFs. Then $A_{2/3}$ is block diagonal with block partitioning

$$\pi_{2/3} = \left\{ \bigcup_{c \in C_0} \check{c}, \bigcup_{c \in C_{1/3}} \check{c}, w_{2/3} \right\}.$$

Level 2/3. Defined at this point are $A_{2/3}$ and $w_{2/3}$, with the active DOFs lying along the edges of the cubes of width mh . We construct a Voronoi diagram on the edge centers. The resulting cells partition $w_{2/3}$ into a disjoint collection $C_{2/3} = \{c\}$, where each c is the set of active DOFs of one such cell. Clearly, $\bigcup_{c \in C_{2/3}} c = w_{2/3}$. Skeletonization with respect to $C_{2/3}$ then yields

$$A_1 = \mathcal{Z}_{2/3}(A_{2/3}) \approx U_{2/3}^* A_{2/3} V_{2/3}, \quad U_{2/3} = \prod_{c \in C_{2/3}} Q_c R_c, \quad V_{2/3} = \prod_{c \in C_{2/3}} Q_c S_c,$$

where the DOFs $\bigcup_{c \in C_{2/3}} \check{c}$ have been decoupled. Let $w_1 = w_{2/3} \setminus \bigcup_{c \in C_{2/3}} \check{c} = \bigcup_{c \in C_{2/3}} \hat{c}$ be the remaining active DOFs. Then A_1 is block diagonal with block partitioning

$$\pi_1 = \left\{ \bigcup_{c \in C_0} \check{c}, \bigcup_{c \in C_{1/3}} \check{c}, \bigcup_{c \in C_{2/3}} \check{c}, w_1 \right\}.$$

Level ℓ . Defined at this point are A_ℓ and w_ℓ . There are $2^{L-\ell} \times 2^{L-\ell} \times 2^{L-\ell}$ cubes of width $2^\ell mh$. Let $C_\ell = \{c\}$ be the disjoint collection of the active DOFs c of each cube. Clearly, $\bigcup_{c \in C_\ell} c = w_\ell$. Skeletonization with respect to C_ℓ gives

$$A_{\ell+1/3} = \mathcal{Z}_\ell(A_\ell) \approx U_\ell^* A_\ell V_\ell, \quad U_\ell = \prod_{c \in C_\ell} Q_c R_c, \quad V_\ell = \prod_{c \in C_\ell} Q_c S_c,$$

where the DOFs $\bigcup_{c \in C_\ell} \check{c}$ have been decoupled. The matrix $A_{\ell+1/3}$ is block diagonal with block partitioning

$$\pi_{\ell+1/3} = \left\{ \bigcup_{c \in C_0} \check{c}, \bigcup_{c \in C_{1/3}} \check{c}, \dots, \bigcup_{c \in C_\ell} \check{c}, w_{\ell+1/3} \right\},$$

where $w_{\ell+1/3} = w_\ell \setminus \bigcup_{c \in C_\ell} \check{c} = \bigcup_{c \in C_\ell} \hat{c}$.

Level $\ell + 1/3$. Defined at this point are $A_{\ell+1/3}$ and $w_{\ell+1/3}$. We construct a Voronoi diagram on the centers of the faces of the cubes of width $2^\ell mh$. The resulting cells partition $w_{\ell+1/3}$ into a disjoint collection $C_{\ell+1/3} = \{c\}$, where each c is the set of active DOFs of one such cell. Clearly, $\bigcup_{c \in C_{\ell+1/3}} = w_{\ell+1/3}$. Skeletonization with respect to $C_{\ell+1/3}$ gives

$$A_{\ell+2/3} = \mathcal{Z}_{\ell+1/3}(A_{\ell+1/3}) \approx U_{\ell+1/3}^* A_{\ell+1/3} V_{\ell+1/3}, \quad U_{\ell+1/3} = \prod_{c \in C_{\ell+1/3}} Q_c R_c, \quad V_{\ell+1/3} = \prod_{c \in C_{\ell+1/3}} Q_c S_c,$$

where the DOFs $\bigcup_{c \in C_{\ell+1/3}} \check{c}$ have been decoupled. The matrix $A_{\ell+2/3}$ is block diagonal with block partitioning

$$\pi_{\ell+2/3} = \left\{ \bigcup_{c \in C_0} \check{c}, \bigcup_{c \in C_{1/3}} \check{c}, \dots, \bigcup_{c \in C_{\ell+1/3}} \check{c}, w_{\ell+2/3} \right\},$$

where $w_{\ell+2/3} = w_{\ell+1/3} \setminus \bigcup_{c \in C_{\ell+1/3}} \check{c} = \bigcup_{c \in C_{\ell+1/3}} \hat{c}$.

Level $\ell + 2/3$. Defined at this point are $A_{\ell+2/3}$ and $w_{\ell+2/3}$. We construct a Voronoi diagram on the centers of the edges of the cubes of width $2^\ell mh$. The resulting cells partition $w_{\ell+2/3}$ into a disjoint collection $C_{\ell+2/3} = \{c\}$, where each c is the set of active DOFs of one such cell. Clearly, $\bigcup_{c \in C_{\ell+2/3}} = w_{\ell+2/3}$. Skeletonization with respect to $C_{\ell+2/3}$ gives

$$A_{\ell+1} = \mathcal{Z}_{\ell+2/3}(A_{\ell+2/3}) \approx U_{\ell+2/3}^* A_{\ell+2/3} V_{\ell+2/3}, \quad U_{\ell+2/3} = \prod_{c \in C_{\ell+2/3}} Q_c R_c, \quad V_{\ell+2/3} = \prod_{c \in C_{\ell+2/3}} Q_c S_c,$$

where the DOFs $\bigcup_{c \in C_{\ell+2/3}} \check{c}$ have been decoupled. The matrix $A_{\ell+1}$ is block diagonal with block partitioning

$$\pi_{\ell+1} = \left\{ \bigcup_{c \in C_0} \check{c}, \bigcup_{c \in C_{1/3}} \check{c}, \dots, \bigcup_{c \in C_{\ell+2/3}} \check{c}, w_{\ell+1} \right\},$$

where $w_{\ell+1} = w_{\ell+2/3} \setminus \bigcup_{c \in C_{\ell+2/3}} \check{c} = \bigcup_{c \in C_{\ell+2/3}} \hat{c}$.

Level L . Finally, we have A_L and w_L , where $D \equiv A_L$ is block diagonal with block partitioning

$$\pi_L = \left\{ \bigcup_{c \in C_0} \check{c}, \bigcup_{c \in C_{1/3}} \check{c}, \dots, \bigcup_{c \in C_{L-1/3}} \check{c}, w_L \right\}.$$

Combining the approximation over all levels gives

$$D \approx U_{L-1/3}^* \cdots U_{1/3}^* U_0^* A V_0 V_{1/3} \cdots V_{L-1/3},$$

so

$$(3.2a) \quad A \approx U_0^{-*} U_{1/3}^{-*} \cdots U_{L-1/3}^{-*} D V_{L-1/3}^{-1} \cdots V_{1/3}^{-1} V_0^{-1} \equiv F,$$

$$(3.2b) \quad A^{-1} \approx V_0 V_{1/3} \cdots V_{L-1/3} D^{-1} U_{L-1/3}^* \cdots U_{1/3}^* U_0^* = F^{-1}.$$

3.3. Accelerated compression. The dominant cost of constructing the HIF is in computing the ID, which for an $m \times n$ matrix of rank k requires $\mathcal{O}(kmn)$ operations [13]. For k , m , and n large, this can be very expensive. Thus, it is imperative to reduce the matrix size as much as possible. Consider any DOF set $c \in C_\ell$ encountered during the algorithm and let $x = \text{ctr}(c)$ be the center about which it is based. For convenience, we also let $\text{ctr}(c')$ for a given DOF c' denote the center of the DOF set to which it belongs. Then rescaling for simplicity so that $2^\ell m h = 1$, c^C admits the partitioning $c^C = c^N \cup c^F$, where

$$c^N = \{c' \in c^C : \|x - y\|_\infty \leq 1, y = \text{ctr}(c')\}$$

is the *neighbor set* of c , consisting of the DOFs with immediately adjacent centers, and c^F is the so-called far field. Correspondingly, the off-diagonal matrix block $A_{c^C, c}$ can be written as

$$A_{c^C, c} = \begin{bmatrix} A_{c^N, c} \\ A_{c^F, c} \end{bmatrix}.$$

We describe two strategies for reducing the size of $A_{c^C, c}$. The first is based on the ellipticity of the underlying PDE. It is easiest to consider the case $b(x) \equiv c(x) \equiv 1$ with $K(r)$ harmonic. Then by Green's theorem, any interaction with c^F can be represented by interactions with the interface Γ separating c^N and c^F . Since Γ is well-separated from c , it requires only a fixed number of DOFs to discretize to a given precision [25, 26, 29, 30]. Denote these DOFs by \tilde{c}^F , which have variously been called *equivalent densities* or *proxy points* [13, 15, 22, 24, 35, 39, 40, 51, 52]. In linear algebraic terms, we hence have $A_{c^F, c} \approx U_c^F A_{\tilde{c}^F, c}$ for some U_c^F . Therefore, $A_{c^C, c}$ has a low-rank decomposition

$$A_{c^C, c} \approx \begin{bmatrix} I \\ U_c^F \end{bmatrix} B_c, \quad B_c = \begin{bmatrix} A_{c^N, c} \\ A_{\tilde{c}^F, c} \end{bmatrix},$$

so it suffices to compute an ID of the much smaller matrix B_c . Notice that $|c^F| = \mathcal{O}(N)$ while $|\tilde{c}^F| = \mathcal{O}(1)$. This procedure thus transforms a fully global operation into a purely local one. The use of equivalent far-field DOFs is critical to achieving linear complexity.

The interface Γ between c^N and c^F can be complicated, especially at fractional levels. Fortunately, any Γ contained in the region between c and c^F can be used, provided that it is sufficiently separated from c . In this paper, we use a circle in 2D and a cube in 3D.

Remark 3.2. Note that all DOFs in c^C with modified interactions with respect to c are contained in c^N . Therefore, c interacts with c^F only via the original kernel, over which we have analytic control.

Remark 3.3. This approach can be extended to the case of real analytic kernels [51] and, practically, to any asymptotically smooth kernel as well [40].

The second strategy is based on finding an analogous set of equivalent near-field DOFs \tilde{c}^N by appropriately subselecting c^N . In our experiments, we have found the following to be effective. Sort the DOFs c^N by distance from $\text{ctr}(c)$ and keep only the closest $2|c|$ of them. Then numerically, $A_{c^N, c} \approx U_c^N A_{\tilde{c}^N, c}$ for some U_c^N , so combining with the above,

$$A_{c^C, c} \approx \begin{bmatrix} U_c^N \\ U_c^F \end{bmatrix} B_c, \quad B_c = \begin{bmatrix} A_{\tilde{c}^N, c} \\ A_{\tilde{c}^F, c} \end{bmatrix}.$$

The ID is now to be computed for B_c . This substantially reduces the constant associated with skeletonization, especially in 3D. It is possible [15] to further subselect until $|\hat{c}^N| = \rho|c|$, for $1 \leq \rho < 2$, particularly when only low precision is required. The choice $\rho = 2$, though, provides a good compromise between accuracy and speed.

Although not presently implemented, another idea when there is sufficient regularity is to simply choose the skeleton DOFs \hat{c} a priori and then perform a least squares solve for T_c [13]. This was carried out to some extent in [15]. The least squares solve can be done densely if $|\hat{c}|$ is small or even in compressed form if $|\hat{c}|$ is large [3, 17, 34].

3.4. Complexity analysis. We now consider the computational complexity of the HIF. For this, we need to estimate the skeleton size $|\hat{c}|$ for a typical DOF set $c \in C_\ell$ at each level $0 \leq \ell \leq L$. Consider first just the levels $\ell \in \mathbb{N}+1/2$ in 2D and $\ell \in \mathbb{N}+2/3$ in 3D corresponding to skeletonization on edges. Then provided that c interacts with c^C via an elliptic kernel, it can be shown that $|\hat{c}| = \mathcal{O}(\log n_\ell) = \mathcal{O}(\ell)$, where $n_\ell = \mathcal{O}(2^\ell)$ is the number of DOFs covering an edge at level ℓ [24, 35]. Extensive numerical experiments [15] and physical intuition suggest that the same is also true of the modified kernels above. Therefore, we assume that $|\hat{c}| = \mathcal{O}(\ell)$ for all $\ell \in \mathbb{N} - 1/d$.

Consider now a square in 2D with DOF set c at any level $\ell \geq 1$. Clearly, c is obtained by combining active DOFs from a fixed number of edges at level $\ell - 1/2$. Thus, $|c| = \mathcal{O}(\ell)$ hence $|\hat{c}| = \mathcal{O}(\ell)$ as well. A similar argument applies in 3D. In summary, we have $|\hat{c}| = \mathcal{O}(\ell)$ for all $\ell \geq 1 - 1/d$ with $|\hat{c}| = \mathcal{O}(1)$ otherwise. The constant implicit in this expression likely has the form $\mathcal{O}(2^d \log(1/\epsilon))$, i.e., it is exponential in the dimension and logarithmic in the precision.

Theorem 3.4. *In both 2D and 3D, corresponding to the factorization F in (3.1) and (3.2), respectively, the costs of constructing F , storing F , applying F , and applying F^{-1} are all $\mathcal{O}(N)$.*

Proof. Let d be the dimension of the problem. Then the cost of constructing F using the acceleration techniques of Section 3.3 is

$$t_f = \sum_{\ell} 2^{d(L-\ell)} \mathcal{O}(|\hat{c}|^3) = \mathcal{O}(2^{dL}) = \mathcal{O}(N)$$

for both $d = 2$ and 3 , where the sum is taken over all integer and fractional levels. Similarly, the cost of storing F is

$$m_f = \sum_{\ell} 2^{d(L-\ell)} \mathcal{O}(|\hat{c}|^2) = \mathcal{O}(2^{dL}) = \mathcal{O}(N).$$

The costs of applying both F and F^{-1} are clearly the same as the memory cost m_f , provided, e.g., that the block diagonal matrix D is stored in factored form. \square

Remark 3.5. As in RS, the prefactor for applying F or F^{-1} is orders of magnitude smaller than that for constructing F . Therefore, a given precomputed factorization enables the repeated calculation of matrix-vector products or linear solves in an extremely efficiently manner.

Remark 3.6. In 2D, if $|\hat{c}| = \mathcal{O}(2^{2\ell/3})$, then $t_f = \mathcal{O}(N \log N)$ with the other quantities scaling as $\mathcal{O}(N)$. The same conclusion is reached in 3D if $|\hat{c}| = \mathcal{O}(2^\ell)$. For any slower growth rate, e.g., $|\hat{c}| = \mathcal{O}(\ell)$, all costs are $\mathcal{O}(N)$.

4. NUMERICAL RESULTS

In this section, we demonstrate the practical efficiency of the HIF by reporting some numerical results in 2D and 3D. All algorithms are implemented in MATLAB R2012b (The MathWorks, Inc.: Natick, MA). In each case, the following, if applicable, are given:

TABLE 4.1. Numerical results for Example 1.

ϵ	N	$ \hat{c} $	m_f (GB)	t_f (s)	$t_{a/s}$ (s)	e_a	e_s	n_i
10^{-3}	256^2	19	$9.8e-2$	$1.0e+1$	$1.6e-1$	$1.8e-04$	$1.1e-2$	8
	512^2	20	$3.8e-1$	$4.3e+1$	$6.3e-1$	$1.6e-04$	$1.6e-2$	8
	1024^2	20	$1.5e+0$	$1.8e+2$	$2.6e+0$	$2.1e-04$	$1.4e-2$	9
	2048^2	21	$6.1e+0$	$7.5e+2$	$1.1e+1$	$2.2e-04$	$3.4e-2$	9
10^{-6}	256^2	85	$3.0e-1$	$2.7e+1$	$1.2e-1$	$2.0e-07$	$1.6e-5$	3
	512^2	99	$1.3e+0$	$1.3e+2$	$5.0e-1$	$1.3e-07$	$2.3e-5$	3
	1024^2	115	$5.4e+0$	$5.9e+2$	$2.1e+0$	$2.5e-07$	$3.4e-5$	3
10^{-9}	256^2	132	$4.4e-1$	$4.5e+1$	$1.2e-1$	$7.8e-11$	$1.3e-8$	2
	512^2	155	$1.8e+0$	$2.1e+2$	$4.9e-1$	$1.1e-10$	$1.6e-8$	2
	1024^2	181	$7.5e+0$	$9.7e+2$	$2.0e+0$	$1.8e-10$	$3.1e-8$	2

- ϵ : the relative precision of the ID, i.e., the local error of approximation for skeletonization;
- N : the total number of DOFs of the problem;
- $|\hat{c}|$: the average size of the skeleton set of an edge at the highest level;
- m_f : the memory required to store the factorization F in GB;
- t_f : the wall clock time for constructing F in seconds;
- $t_{a/s}$: the wall clock time for applying F or F^{-1} in seconds;
- e_a : the relative error $\|(A - F)f\|/\|Af\|$ of applying F to a vector f with uniform random entries, estimated by computing the norm over a random selection of 128 entries;
- e_s : the relative residual $\|AF^{-1}f\|/\|f\|$ of applying F^{-1} to a vector f with uniform random entries, estimated by computing the norm over a random selection of 128 entries; and
- n_i : the number of iterations to solve $Au = f$ using GMRES with preconditioner F^{-1} to a tolerance of 10^{-12} , where f has uniform random entries (first-kind integral equations only).

All integral equations are discretized using a piecewise constant collocation method as in Section 3. The block size $|c|$ at level 0 is chosen adaptively to optimize the running time. In certain cases, the first few levels of dimensional reduction are skipped because they do not produce sufficient compression. For examples on regular grids requiring iteration, A is applied using fast Fourier convolutional methods [7]. All computations are run in serial on a single core of a 64-bit Linux desktop with 3.6 GHz CPUs and 36 GB of RAM.

For the sake of generality, we do not exploit symmetry in any of the examples below. Specifically, in all but Example 3, the factorization time t_f can be reduced by roughly a factor of 2 by applying the ID only to, say, $A_{p^c,p}$ instead of both $A_{p^c,p}$ and A_{p,p^c}^* as in Section 2.4.

4.1. Two dimensions. We begin first in 2D, where we present three examples.

Example 1. Consider the integral equation (1.1) with $a(x) \equiv 0$, $b(x) \equiv c(x) \equiv 1$, $K(r) = -1/(2\pi) \log r$, and $\Omega = (0, 1)^2$, i.e., a first-kind integral equation in the unit square. The results are summarized in Table 4.1. It is evident that for fixed ϵ , $|\hat{c}| = \mathcal{O}(\log N) = \mathcal{O}(L)$, which is consistent with the assumptions of Theorem 3.4. Furthermore, for fixed N , $|\hat{c}|$ appears to grow as $|\hat{c}| = \mathcal{O}(\log(1/\epsilon))$ as predicted. Therefore, the price of a more accurate factorization is a moderate increase in $|\hat{c}|$ and hence in m_f , t_f , and $t_{a/s}$. The data moreover clearly show that each of these quantities scales essentially as $\mathcal{O}(N)$ in support of Theorem 3.4.

TABLE 4.2. Numerical results for Example 2.

ϵ	N	$ \hat{c} $	m_f (GB)	t_f (s)	$t_{a/s}$ (s)	e_a	e_s
10^{-8}	256^2	186	$4.8\text{e}-1$	$5.6\text{e}+1$	$1.2\text{e}-1$	$9.2\text{e}-10$	$9.1\text{e}-10$
	512^2	275	$2.2\text{e}+0$	$3.4\text{e}+2$	$5.1\text{e}-1$	$4.5\text{e}-09$	$4.4\text{e}-09$
	1024^2	325	$9.7\text{e}+0$	$1.7\text{e}+3$	$2.1\text{e}+0$	$3.6\text{e}-08$	$3.5\text{e}-08$

Timing profiles reveal that the main contribution to $t_{a/s}$ is memory access, leading to the peculiar observation that $t_{a/s}$ remains basically unchanged from $\epsilon = 10^{-6}$ to 10^{-9} . In fact, $t_{a/s}$ is largest for $\epsilon = 10^{-3}$. This is due to the fact that the HIF employs additional levels of skeletonization in this case because a smaller level 0 block size can be used.

The application error e_a is always smaller than ϵ , though it seems to increase slowly with N . This suggests that the accuracy of the ID provides a good estimate of the overall accuracy of the HIF. On the other hand, the residual e_s is much larger due to the ill conditioning of the problem. When using F^{-1} to precondition GMRES, however, the number n_i of iterations required is always very small. This indicates that F^{-1} is a highly effective preconditioner.

Compared to a similarly implemented RS code, which scales quite robustly as $\mathcal{O}(N^{3/2})$, the HIF is initially slower due to the additional overhead but breaks even at $N \sim 20000$ for $\epsilon = 10^{-3}$ and $N \sim 5000$ for $\epsilon = 10^{-6}$ and 10^{-9} . In all cases, the memory usage of the HIF is lower than that of RS. At $N = 1024^2$ and $\epsilon = 10^{-9}$, for instance, the HIF has $m_f = 7.5$ GB while RS has $m_f = 17.0$ GB. The final skeleton matrix size, of course, is much smaller: $|w_L| = 4|\hat{c}| = 722$ for the HIF vs. $|w_L| = 8295$ for RS. For the same example at $\epsilon = 10^{-3}$, these become just $m_f = 1.5$ GB and $|w_L| = 80$ for the HIF vs. $m_f = 5.4$ GB and $|w_L| = 4113$ for RS. In all cases, $t_{a/s}$ is very similar for both algorithms.

Example 2. Now consider (1.1) with $a(x) \equiv b(x) \equiv c(x) \equiv 1$, $K(r) = -1/(2\pi) \log r$, and $\Omega = (0, 1)^2$. This is a well-conditioned second-kind integral equation so we expect that F^{-1} can provide an accurate solution directly without iteration. The results are summarized in Table 4.2. As before, $|\hat{c}|$ scales roughly as $\mathcal{O}(\log N)$ with m_f , t_f , and $t_{a/s}$ all increasing essentially linearly. Both e_a and e_s are of order $\mathcal{O}(\epsilon)$ but grow somewhat with N .

Note that $|\hat{c}|$ is much larger here than in Example 1. This is because the matrices compressed by the ID tend to be, rather surprisingly, more ill-conditioned than in the first-kind case. The origin of this oddity can be seen as follows. Let A as in (2.2) be a typical second-kind integral equation matrix discretization. Then the diagonal entries of A are $\mathcal{O}(1)$ but its off-diagonal entries are $\mathcal{O}(1/N)$. The interpolation matrix, say, T_p from the ID also has entries of order $\mathcal{O}(1)$, so the entries of the matrices $B_{\hat{p}\hat{p}}$, $B_{\hat{p}\hat{p}}$, and $B_{\hat{p}\hat{p}}$ in (2.3) are all $\mathcal{O}(1)$ as well. Hence the nonzeros of the Schur complement matrices (2.4) are $\mathcal{O}(1)$ and the same is true of the modified kernel $B_{\hat{p}\hat{p}}$ in (2.5). Therefore, on moving to the next level, the $\mathcal{O}(1)$ modified kernel is mixed with the $\mathcal{O}(1/N)$ original kernel, leading to a matrix with vastly different scales.

As a result, it is very important to compute the ID accurately. In our tests, we have found the standard algorithm based on the pivoted QR factorization with a relative pivot threshold of ϵ to be insufficient. Thus, we supplement it with a randomized power method [18, 37] to estimate the approximation error and an adaptive scheme using the thresholds $\epsilon, \epsilon/2, \epsilon/4, \dots$ in succession until the desired accuracy is achieved. This iteration often converges in no more than one or two steps, so the overhead is modest.

TABLE 4.3. Numerical results for Example 3.

ϵ	N	$ \hat{c} $	m_f (GB)	t_f (s)	$t_{a/s}$ (s)	e_a	e_s
10^{-8}	256^2	404	1.1e+0	1.8e+2	1.3e-1	4.1e-9	4.1e-9
	512^2	527	4.6e+0	9.5e+2	5.7e-1	1.9e-8	1.9e-8
	1024^2	607	1.7e+1	3.7e+3	2.1e+0	4.8e-8	4.8e-8

TABLE 4.4. Numerical results for Example 4.

ϵ	N	$ \hat{c} $	m_f (GB)	t_f (s)	$t_{a/s}$ (s)	e_a	e_s
10^{-3}	20480	201	1.4e-1	9.8e+0	3.8e-2	7.2e-4	7.1e-4
	81920	307	5.6e-1	5.0e+1	1.8e-1	1.8e-3	1.8e-3
	327680	373	2.1e+0	2.2e+2	7.5e-1	3.8e-3	3.7e-3
	1310720	440	8.1e+0	8.9e+2	3.2e+0	9.7e-3	9.5e-3
10^{-6}	20480	497	5.2e-1	6.3e+1	5.3e-2	1.1e-7	1.1e-7
	81920	841	2.1e+0	4.1e+2	2.4e-1	2.3e-7	2.3e-7
	327680	1236	8.2e+0	2.3e+3	1.0e+0	1.2e-6	1.2e-6

The HIF breaks even with RS at $N \sim 15000$. As in Example 1, it always uses less memory, with $m_f = 9.7$ GB and $|w_L| = 1300$ at $N = 1024^2$ vs. $m_f = 16.6$ GB and $|w_L| = 8229$ for RS. There is no substantial difference in $t_{a/s}$.

Example 3. Consider now a variable-coefficient second-kind integral equation by taking (1.1) with $a(x) \equiv 1$, $b(x) = b(x_1, x_2) = \exp(-16((x_1 - 1/2)^2 + (x_2 - 1/2)^2))$, $c(x) = c(x_1, x_2) = \sin(3\pi x_2)$, $K(r) = -1/(2\pi) \log r$, and $\Omega = (0, 1)^2$. The coefficient functions are smooth but somewhat rapidly varying, with b having local support and c vanishing along lines. The results are summarized in Table 4.3 and are qualitatively similar to those of Example 2 but with larger ranks $|\hat{c}|$ to account for the increased complexity of the problem. The HIF now breaks even with RS at $N \sim 20000$. We note that RS runs out of memory during factorization at $N = 1024^2$.

4.2. Three dimensions. We next present two examples in 3D: a boundary integral equation on the sphere and a volume integral equation in the cube.

Example 4. Consider the integral equation (1.1) with $a(x) \equiv b(x) \equiv c(x) \equiv 1$, $K(r) = 1/(4\pi r)$, and $\Omega = S^2$ the unit sphere. This is a second-kind boundary integral equation similar to that associated with the Dirichlet Laplace problem (1.2), cf. (1.5). It is possible to reparametrize Ω in 2D and then use the 2D algorithm, but we use the full 3D solver here. Since Ω is no longer regular, we use an adaptive octree [46] to hierarchically partition the domain. This is done by first enclosing all DOFs within a sufficiently large box. If the box contains more than a set number of DOFs, it is subdivided into eight equal orthants and its DOFs split between them accordingly. This is repeated for each new box added, with the overall procedure terminating when all leaf boxes contain $\mathcal{O}(1)$ DOFs. Only non-empty boxes are retained throughout.

Because of adaptivity, different leaf boxes can be on different levels of the tree. However, this presents no difficulty and the HIF can be applied without modification, with each box being skeletonized as the algorithm reaches its level as it marches up the tree.

Numerical results are summarized in Table 4.4. As in 2D, we observe that $|\hat{c}| = \mathcal{O}(\log N)$ for fixed ϵ . The scaling with ϵ for fixed N , however, is much less clear. Still, the ratio of $m_f = \mathcal{O}(|\hat{c}|^2)$

TABLE 4.5. Numerical results for Example 5.

ϵ	N	$ \hat{c} $	m_f	t_f	$t_{a/s}$	e_a	e_s	n_i
10^{-2}	16^3	39	1.5e-2	1.5e+0	1.5e-2	6.0e-3	2.8e-2	10
	32^3	51	1.7e-1	2.1e+1	1.5e-1	9.0e-3	5.7e-2	14
	64^3	65	1.7e+0	2.8e+2	1.4e+0	1.3e-2	1.3e-1	17
10^{-3}	16^3	92	4.3e-2	2.7e+0	9.6e-3	2.2e-4	1.0e-3	6
	32^3	171	4.1e-1	4.8e+1	5.9e-2	4.0e-4	2.0e-3	8
	64^3	364	4.2e+0	8.8e+2	5.7e-1	7.1e-4	2.4e-3	8
10^{-4}	16^3	182	6.1e-2	3.1e+0	7.2e-3	1.2e-5	1.2e-4	4
	32^3	360	7.7e-1	1.5e+2	8.6e-2	2.8e-5	2.3e-4	5
	64^3	793	9.1e+0	3.5e+3	9.1e-1	5.7e-5	3.6e-4	5

at $\epsilon = 10^{-6}$ to that at $\epsilon = 10^{-3}$ is about 4 at each N , which is consistent with the estimate $|\hat{c}| = \mathcal{O}(\log(1/\epsilon))$. Similarly, the ratio of $t_f = \mathcal{O}(|\hat{c}|^3)$ is about 8. We remark that we do not see this behavior in Example 1, most likely because $|\hat{c}|$ is small in that case so that other constants dominate. Approximately linear growth of m_f , t_f , and $t_{a/s}$ is observed. Both e_a and e_s are of order $\mathcal{O}(\epsilon)$ but increase somewhat with N .

Compared to RS, which scales as $\mathcal{O}(N^{3/2})$ since the true dimension of the problem is $d = 2$, the HIF breaks even at $N \sim 20000$ for both $\epsilon = 10^{-3}$ and 10^{-6} . The memory usage is always lower, with $m_f = 8.2$ GB and $|w_L| = 6|\hat{c}| = 7414$ at $N = 327680$ and $\epsilon = 10^{-6}$ vs. $m_f = 16.7$ GB and $|w_L| = 16718$ for RS. At $\epsilon = 10^{-3}$, these become just $m_f = 2.1$ GB and $|w_L| = 2239$ for the HIF vs. $m_f = 5.0$ GB and $|w_L| = 8630$ for RS. There is no substantial difference in $t_{a/s}$.

Remark 4.1. Although building the octree is formally an $\mathcal{O}(N \log N)$ process, in practice it is an almost imperceptible part of the overall algorithm, requiring no more than a few seconds on even the largest problems examined.

Example 5. Finally, we consider (1.1) with $a(x) \equiv 0$, $b(x) \equiv c(x) \equiv 1$, $K(r) = 1/(4\pi r)$, and $\Omega = (0, 1)^3$. The results are summarized in Table 4.5. For $\epsilon = 10^{-2}$, the algorithm scales close to linearly, with $|\hat{c}| = \mathcal{O}(\log N)$ as predicted. For $\epsilon = 10^{-3}$ or 10^{-4} , however, the growth is slightly larger, with an increase in t_f by a factor of about 20 when N increases by a factor of 8. This can be explained by observing that we have not yet reached the asymptotic regime. In particular, the number of levels at $N = 16^3$, 32^3 , and 64^3 , respectively, is only $L = 1, 2$, and 3 . For comparison, the HIF at $\epsilon = 10^{-2}$ has $L = 2, 3$, and 4 , respectively, which also explains the increase in $t_{a/s}$ when considered in conjunction with the memory access bottleneck described in Example 1. Furthermore, there are proportionally more boundary cubes, which require less work, when L is small. Nonetheless, this is still significantly better than the expected factor increase of 64 using RS or 512 using classical direct methods. Indeed, the corresponding factor increase observed for RS is actually closer to 100. We moreover note that for $\epsilon = 10^{-3}$ and 10^{-4} , $|\hat{c}|$ seems to grow as $\mathcal{O}(2^\ell)$. Although we expect that $|\hat{c}| = \mathcal{O}(\ell)$ asymptotically, even such a scaling would result in an $\mathcal{O}(N \log N)$ algorithm by Remark 3.6.

As in Example 1, $e_a = \mathcal{O}(\epsilon)$ but e_s is somewhat larger due to the ill conditioning of the first-kind system. However, n_i remains small, especially at higher precisions, so that F^{-1} is a very effective preconditioner.

The break-even point with RS is now only $N \sim 5000$ at all ϵ tested. This is because RS scales as $\mathcal{O}(N^2)$ in 3D so that the complexity advantage of the HIF really begins to exert itself. Again,

the memory usage is always lower, with $m_f = 0.7$ GB and $|w_L| = 2159$ at $N = 32^3$ and $\epsilon = 10^{-4}$ vs. $m_f = 1.8$ GB and $|w_L| = 6357$ for RS. At $\epsilon = 10^{-2}$, these become just $m_f = 0.17$ GB and $|w_L| = 307$ for the HIF vs. $m_f = 1.4$ GB and $|w_L| = 5779$ for RS. We note that RS runs out of memory during factorization at $N = 64^3$ for all ϵ . Furthermore, it can now clearly be seen that $t_{a/s} = \mathcal{O}(N^{4/3})$ for RS; $t_{a/s}$ breaks even also at $N \sim 5000$.

5. GENERALIZATIONS AND CONCLUSIONS

In this paper, we have introduced the HIF for matrices arising from integral equations associated with elliptic PDEs in 2D and 3D. The HIF is a novel matrix factorization that follows the general structure of RS but uses additional levels of skeletonization to recursively reduce the dimension of the skeleton set and hence to control the rank growth. The resulting skeleton sizes scale as $\mathcal{O}(\log N)$, leading to memory, factorization, application, and solve costs of $\mathcal{O}(N)$ as shown both analytically and numerically, at least in 2D. In 3D, the results are somewhat inconclusive, but there is strong evidence that the cost is either $\mathcal{O}(N)$ or $\mathcal{O}(N \log N)$. The overall accuracy of the HIF is controlled by the accuracy ϵ of the ID. Due to its multiplicative form, the HIF can be used variously as an FMM, direct solver (if ϵ is small), or preconditioner (if ϵ is not so small).

Unlike [15], which exploited a nested hierarchical structure to achieve $\mathcal{O}(N)$ complexity in 2D, the HIF uses only a single pseudo-hierarchy to do so in both 2D and 3D. This makes the algorithm considerably simpler and easier to implement. It further obviates the need for hierarchical matrix arithmetic, relying instead only on well-optimized dense matrix routines.

Although we have presently targeted the HIF to integral equations, the same algorithm can be applied without modification to the PDE itself when discretized using local schemes such as finite differences or finite elements. In this setting, many off-diagonal blocks are trivially low-rank since each DOF only interacts with its immediate neighbors. Consequently, the skeleton sizes tend to be much smaller [36], but the inherent ill conditioning of the PDE system can degrade the solution accuracy. Furthermore, the current algorithm does not exploit sparsity. Therefore, the HIF can be heavily optimized for the PDE case; for results in this direction, we refer the reader to the companion paper [36].

There are several alternative ways to interpret the HIF. For example, we can view it as an approximate change of basis of the elliptic operator in order to gain sparsity. In contrast to the traditional approach, however, the basis here is determined optimally on the fly via the ID. We can also view the HIF as a special multigrid method, again with the prolongation and restriction operators chosen adaptively to decimate as many DOFs as possible.

Several clear directions for future research are available, just to name a few. First, an analytical estimate of the skeleton size $|\hat{c}|$, even for the simple case of the Laplace kernel (1.4), would enable a much more precise understanding of the complexities of the proposed algorithms. This is, however, not so easy as the ID is not quite amenable to rigorous analysis. Second, the HIF can be applied to Helmholtz and Maxwell problems to study scattering, a central topic in modern mathematical physics [14]. Based on results for other skeletonization schemes [15, 35, 39], we expect that it will be effective at low and moderate frequencies. The high-frequency regime, however, seems to require new ideas. Third, the HIF has significant potential for parallelization, especially since the skeleton matrices have markedly reduced sizes. Finally and perhaps most importantly, we hope that the HIF has demonstrated the utility of the ID, which is still a relatively new and unused tool in numerical linear algebra. We anticipate that the ID will catalyze the development of powerful new fast multiscale algorithms as it already has in this setting and others [4, 8, 20, 21, 36, 42, 47].

Acknowledgements. We would like to thank Leslie Greengard for many helpful discussions. K.L.H. was partially supported by the National Science Foundation under award DMS-1203554. L.Y. was partially supported by the National Science Foundation under award DMS-0846501 and the U.S. Department of Energy’s Advanced Scientific Computing Research program under award DE-FC02-13ER26134/DE-SC0009409.

REFERENCES

- [1] Ambikasaran, S.; Darve, E. An $\mathcal{O}(N \log N)$ fast direct solver for partial hierarchically semi-separable matrices. *J. Sci. Comput.*, doi:10.1007/s10915-013-9714-z.
- [2] Barnes, J.; Hut, P. A hierarchical $\mathcal{O}(N \log N)$ force-calculation algorithm. *Nature* **324** (1986), no. 4, 446–449.
- [3] Benner, P.; Mach, T. On the QR decomposition of \mathcal{H} -matrices. *Computing* **88** (2010), no. 3–4, 111–129.
- [4] Bermanis, A.; Averbuch, A.; Coifman, R. R. Multiscale data sampling and function extension. *Appl. Comput. Harmon. Anal.* **34** (2013), no. 1, 15–29.
- [5] Börm, S. *Efficient numerical methods for non-local operators. \mathcal{H}^2 -matrix compression, algorithms and analysis.* European Mathematical Society, Zurich, 2010.
- [6] Bremer, J. A fast direct solver for the integral equations of scattering theory on planar curves with corners. *J. Comput. Phys.* **231** (2012), no. 4, 1879–1899.
- [7] Brigham, E. O. *The Fast Fourier Transform and its applications.* Prentice Hall, Englewood Cliffs, 1988.
- [8] Candès, E.; Demanet, L.; Ying, L. A fast butterfly algorithm for the computation of Fourier integral operators. *Multiscale Model. Simul.* **7** (2009), no. 4, 1727–1750.
- [9] Chan, T. F. Rank revealing QR factorizations. *Linear Algebra Appl.* **88–89** (1987), 67–82.
- [10] Chandrasekaran, S.; Dewilde, P.; Gu, M.; Lyons, W.; Pals, T. A fast solver for HSS representations via sparse matrices. *SIAM J. Matrix Anal. Appl.* **29** (2006), no. 1, 67–81.
- [11] Chandrasekaran, S.; Gu, M.; Pals, T. A fast ULV decomposition solver for hierarchically semiseparable representations. *SIAM J. Matrix Anal. Appl.* **28** (2006), no. 3, 603–622.
- [12] Chen, Y. A fast, direct algorithm for the Lippmann-Schwinger integral equation in two dimensions. *Adv. Comput. Math.* **16** (2002), no. 2–3, 175–190.
- [13] Cheng, H.; Gimbutas, G.; Martinsson, P. G.; Rokhlin, V. On the compression of low rank matrices. *SIAM J. Sci. Comput.* **26** (2005), no. 4, 1389–1404.
- [14] Colton, D.; Kress, R. *Inverse acoustic and electromagnetic scattering.* Applied Mathematical Sciences, vol. 93. Springer-Verlag, Berlin, 1992.
- [15] Corona, E.; Martinsson, P.-G.; Zorin, D. An $\mathcal{O}(N)$ direct solver for integral equations on the plane. arXiv:1303.5466.
- [16] Davis, T. A. *Direct methods for sparse linear systems.* Society for Industrial and Applied Mathematics, Philadelphia, 2006.
- [17] Dewilde, P.; Chandrasekaran, S. A hierarchical semi-separable Moore–Penrose equation solver. In D. Alpay, A. Luger, H. Woracek (eds.), *Wavelets, multiscale systems and hypercomplex analysis*, pp. 69–85. Operator Theory: Advances and Applications, vol. 167. Birkhäuser, Basel, 2006.
- [18] Dixon, J. D. Estimating extremal eigenvalues and condition numbers of matrices. *SIAM J. Numer. Anal.* **20** (1983), no. 4, 812–814.
- [19] Fong, W.; Darve, E. The black-box fast multipole method. *J. Comput. Phys.* **228** (2009), no. 23, 8712–8725.
- [20] Gillman, A.; Martinsson, P. G. A direct solver with $\mathcal{O}(N)$ complexity for variable coefficient elliptic PDEs discretized via a high-order composite spectral collocation method. Submitted.
- [21] Gillman, A.; Martinsson, P. G. An $\mathcal{O}(N)$ algorithm for constructing the solution operator to 2D elliptic boundary value problems in the absence of body loads. arXiv:1302.5995.
- [22] Gillman, A.; Young, P. M.; Martinsson, P.-G. A direct solver with $\mathcal{O}(N)$ complexity for integral equations on one-dimensional domains. *Front. Math. China* **7** (2012), no. 2, 217–247.
- [23] Golub, G. H.; van Loan, C. F. *Matrix computations*, 3rd ed. Johns Hopkins University Press, Baltimore, 1996.
- [24] Greengard, L.; Gueyffier, D.; Martinsson, P.-G.; Rokhlin, V. Fast direct solvers for integral equations in complex three-dimensional domains. *Acta Numer.* **18** (2009), 243–275.
- [25] Greengard, L.; Rokhlin, V. A fast algorithm for particle simulations. *J. Comput. Phys.* **73** (1987), no. 2, 325–348.
- [26] Greengard, L.; Rokhlin, V. A new version of the Fast Multipole Method for the Laplace equation in three dimensions. *Acta Numer.* **6** (1997), 229–269.

- [27] Gu, M.; Eisenstat, S. C. Efficient algorithms for computing a strong rank-revealing QR factorization. *SIAM J. Sci. Comput.* **17** (1996), no. 4, 848–869.
- [28] Guenther, R. B.; Lee, J. W. *Partial differential equations of mathematical physics and integral equations*. Prentice Hall, Englewood Cliffs, 1988.
- [29] Hackbusch, W. A sparse matrix arithmetic based on \mathcal{H} -matrices. Part I: introduction to \mathcal{H} -matrices. *Computing* **62** (1999), no. 2, 89–108.
- [30] Hackbusch, W.; Khoromskij, B. N. A sparse \mathcal{H} -matrix arithmetic. Part II: application to multi-dimensional problems. *Computing* **64** (2000), no. 1, 21–47.
- [31] Hackbusch, W.; Nowak, Z. P. On the fast matrix multiplication in the boundary element method by panel clustering. *Numer. Math.* **54** (1989), no. 4, 463–491.
- [32] Halko, N.; Martinsson, P. G.; Tropp, J. A. Finding structure with randomness: probabilistic algorithms for constructing approximate matrix decompositions. *SIAM Rev.* **53** (2011), no. 2, 217–288.
- [33] Hestenes, M. R.; Stiefel, E. Method of conjugate gradients for solving linear systems. *J. Res. Nat. Bur. Stand.* **49** (1952), no. 6, 409–436.
- [34] Ho, K. L.; Greengard, L. A fast direct least squares algorithm for hierarchically block separable matrices. arXiv:1212.3521.
- [35] Ho, K. L.; Greengard, L. A fast direct solver for structured linear systems by recursive skeletonization. *SIAM J. Sci. Comput.* **34** (2012), no. 5, A2507–A2532.
- [36] Ho, K. L.; Ying, L. Hierarchical interpolative factorization for elliptic operators: differential equations. Submitted.
- [37] Kuczyński, J.; Woźniakowski, H. Estimating the largest eigenvalue by the power and Lanczos algorithms with a random start. *SIAM J. Matrix Anal. Appl.* **13** (1992), no. 4, 1094–1122.
- [38] Liberty, E.; Woolfe, F.; Martinsson, P.-G.; Rokhlin, V.; Tygert, M. Randomized algorithms for the low-rank approximation of matrices. *Proc. Natl. Acad. Sci. U.S.A.* **104** (2007), no. 51, 20167–20172.
- [39] Martinsson, P. G.; Rokhlin, V. A fast direct solver for boundary integral equations in two dimensions. *J. Comput. Phys.* **205** (2005), no. 1, 1–23.
- [40] Martinsson, P. G.; Rokhlin, V. An accelerated kernel-independent fast multipole method in one dimension. *SIAM J. Sci. Comput.* **29** (2007), no. 3, 1160–1178.
- [41] Martinsson, P. G.; Rokhlin, V.; Tygert, M. A randomized algorithm for the decomposition of matrices. *Appl. Comput. Harmon. Anal.* **30** (2011), no. 1, 47–68.
- [42] O’Neil, M.; Woolfe, F.; Rokhlin, V. An algorithm for the rapid evaluation of special function transforms. *Appl. Comput. Harmon. Anal.* **28** (2010), no. 2, 203–226.
- [43] Phillips, J. R.; White, J. K. A precorrected-FFT method for electrostatic analysis of complicated 3-D structures. *IEEE Trans. Computer Aid. Design* **16** (1997), no. 10, 1059–1072.
- [44] Saad, Y. *Iterative methods for sparse linear systems*, 2nd ed. Society for Industrial and Applied Mathematics, Philadelphia, 2003.
- [45] Saad, Y.; Schultz, M. H. GMRES: A generalized minimal residual algorithm for solving nonsymmetric linear systems. *SIAM J. Sci. Stat. Comput.* **7** (1986), no. 3, 856–869.
- [46] Samet, H. The quadtree and related hierarchical data structures. *ACM Comput. Surv.* **16** (1984), no. 2, 187–260.
- [47] Tygert, M. Fast algorithms for spherical harmonic expansions, III. *J. Comput. Phys.* **229** (2010), no. 18, 6181–6192.
- [48] van der Vorst, H. A. Bi-CGSTAB: A fast and smoothly converging variant of Bi-CG for the solution of nonsymmetric linear systems. *SIAM J. Sci. Stat. Comput.* **13** (1992), no. 2, 631–644.
- [49] Woolfe, F.; Liberty, E.; Rokhlin, V.; Tygert, M. A fast randomized algorithm for the approximation of matrices. *Appl. Comput. Harmon. Anal.* **25** (2008), no. 3, 335–366.
- [50] Xia, J.; Chandrasekaran, S.; Gu, M.; Li, X. S. Fast algorithms for hierarchically semiseparable matrices. *Numer. Linear Algebra Appl.* **17** (2010), no. 6, 953–976.
- [51] Ying, L. A kernel independent fast multipole algorithm for radial basis functions. *J. Comput. Phys.* **213** (2006), no. 2, 451–457.
- [52] Ying, L.; Biros, G.; Zorin, D. A kernel-independent adaptive fast multipole algorithm in two and three dimensions. *J. Comput. Phys.* **196** (2004), no. 2, 591–626.

(Kenneth L. Ho) DEPARTMENT OF MATHEMATICS, STANFORD UNIVERSITY
E-mail address: `klho@stanford.edu`

(Lexing Ying) DEPARTMENT OF MATHEMATICS AND INSTITUTE FOR COMPUTATIONAL AND MATHEMATICAL EN-
GINEERING, STANFORD UNIVERSITY
E-mail address: `lexing@math.stanford.edu`